Proceedings of the 2006 IEEE International Conference on Robotics and Automation
Orlando, Florida - May 2006

Image Processing Algorithms for UAV "Sense and Avoid"

Ryan Carnie[1,2], Rodney Walker[1]
[1]Australian Research Centre for Aerospace Automation
Queensland University of Technology
PO Box 2434, Brisbane, QLD 4001, Australia
Email: {r.carnie|ra.walker}@qut.edu.au

Peter Corke[1]
[2]CSIRO ICT Centre
PO Box 883, Kenmore, QLD 4069, Australia
Email: peter.corke@csiro.au

***Abstract* – This research is investigating the feasibility of using computer vision to provide a level of situational awareness suitable for the task of UAV "sense and avoid." This term is used to describe the capability of a UAV to detect airborne traffic and respond with appropriate avoidance maneuvers in order to maintain minimum separation distances. As reflected in regulatory requirements such as FAA Order 7610.4, this capability must demonstrate a level of performance which meets or exceeds that of an equivalent human pilot.**

Presented in this paper is a comparison of two initial image processing algorithms that have been designed to detect small, point-like features (potentially corresponding to distant, collision-course aircraft) from image streams, and a discussion of their detection performance in processing a real-life collision scenario. This performance is compared against the stated benchmark of equivalent human performance, specifically the measured detection times of an alerted human observer.

The two algorithms were used to process a series of image streams featuring real collision-course aircraft against a variety of daytime backgrounds. Preliminary analysis of this data set has yielded encouraging results, achieving first detection times at distances of approximately 6.5km (3.5nmi), which are 35-40% greater than those of the alerted human observer. Comparisons were also drawn between the two separate detection algorithms, and have demonstrated that a new approach designed to increase resilience to image noise achieves a lower rate of false alarms, particularly in tests featuring more sensitive detection thresholds.

Index Terms* – *collision avoidance, UAV, computer vision, target detection, sense and avoid

I. Introduction

One of the greatest challenges facing the introduction of UAVs into unrestricted airspace is the development of a collision avoidance capability that meets the standards provided by a human pilot. Current research in this field has experimented with a variety of sensor technologies, such as radar [1], computer vision [2], transponders [3, 4] and data-link information exchange (e.g. ADS-B [5, 6]). While future technology, particularly the introduction of ADS-B, will facilitate high performance collision avoidance systems, it will also introduce a reliance on external factors such as equipment onboard neighboring aircraft and the integrity of the GNSS constellation. It may therefore be argued that such systems are undesirable as a sole-means of collision avoidance onboard a UAV. Computer vision offers a fully self-contained alternative, or "backup," approach which emulates the "see and avoid" mechanism of a human pilot.

This research is investigating the feasibility of using computer vision to provide robust sensing capabilities suitable for the purpose of UAV collision avoidance. Such an approach must provide a level of performance which is at least equivalent to that of human "see and avoid," as stated in FAA Order 7610.4 [7].

Much research has been published on the topic of automatic target detection using computer vision. Approaches to this problem include spatial techniques, such as mathematical morphology [8, 9], median subtraction filters [10], and high pass filters [11], and temporal-based methods such as 3D matched filtering [12, 13], dynamic programming [14-16] and the recursive max filter [17]. In this paper, a combination of morphological filtering and dynamic programming techniques is implemented.

To date, our research has focused on the development of an image processing "front end" that will serve to extract small, point-like features (potentially corresponding to distant, collision-course aircraft) from image streams. A subsequent tracking algorithm, such as the one proposed by Gandhi [2], can then be used to identify features that exhibit motion and expansion properties corresponding to genuine airborne threats.

To this end, we present a morphological close-minus-open (CMO) filter that is used to extract point-like features from large-scale clutter such as clouds. The output is then passed through a dynamic programming algorithm, enhancing detection performance in images with poor signal to noise ratios. An alternative approach is also presented, whereby the CMO filter was modified in order to retain information regarding the sign of the values of detected features, with the aim of increasing resilience to image noise.

A detailed description of these detection algorithms, and a comparison of their performance in processing a sequence of real-life data, is presented.

II. Image Processing Algorithms

A. Morphological Filtering

Spatial filters based on greyscale morphology are useful for extracting small, point-like features that are present within an image frame, amongst larger scale clutter such as clouds. Such filters are derived from two fundamental operations known as *dilation* and *erosion.*

The dilation of a greyscale image, *I(x,y),* by a morphological *structuring element, S(x,y)* is defined [18] by the equation:

$$I(x,y) \oplus S(x,y) = \max_{(x',y') \in S} \{ I(x-x', y-y') + S(x-x', y-y') \} \qquad (1)$$

Where the ranges of x' and y' are set by the size of the structuring element. Similarly, the erosion of a greyscale image *I(x,y)* by a morphological structuring element *S(x,y)* is defined by the equation:

$$I(x,y) \ominus S(x,y) = \min_{(x',y') \in S} \{I(x-x', y-y') - S(x-x', y-y')\} \quad (2)$$

These two fundamental equations can be combined to form two secondary equations, known as *opening* and *closing*, which are highly useful for target detection applications.

The morphological opening of greyscale image *I(x,y)* by structuring element *S(x,y)* is defined as an erosion followed by a dilation:

$$I \circ S = (I \ominus S) \oplus S \quad (3)$$

Conversely, the morphological closing of greyscale image *I(x,y)* by structuring element *S(x,y)* is defined as a dilation followed by an erosion:

$$I \bullet S = (I \oplus S) \ominus S \quad (4)$$

Conceptually, the morphological opening procedure can be described as the darkening of small bright areas (which are too small to accommodate the given morphological structuring element) to the values of their neighbouring pixels. Conversely, morphological closing is used to brighten small, dark areas to match the values of their neighbours.

Given these basic definitions, it is clear that the difference between an image and its morphological opening is useful for identifying positive (brighter than neighbouring pixels) targets. Accordingly, the difference between a closed image and its original may be used to identify negative (darker) targets. Both of the morphological filters investigated in this paper are based on this concept.

1.) Close-Minus-Open (CMO) Filtering Approach

The first approach implemented was a simple close-minus-open (CMO) filter, as defined in (5), which generates a non-negative response that simultaneously identifies point-like targets of both positive and negative nature.

$$CMO(I,S) = (I \bullet S) - (I \circ S) \quad (5)$$

This implementation was based on the approach suggested by Casasent [8], which takes the minimum response of a pair of CMO filters, using horizontal and vertical 1D slits as structuring elements. This dual-filter approach reduces the probability of false detections due to jagged boundaries on larger scale clutter.

2.) Preserved-Sign (PS) Filtering Approach

While the CMO approach is attractive due to its relative simplicity, its output is non-negative in nature and thus false responses generated by zero-mean image noise are no longer characterised by a zero mean. This reduces the effectiveness of the subsequent temporal averaging process using dynamic programming. For this reason, an alternative approach was implemented and compared against the performance of the CMO algorithm.

The new approach adds the differences between the image frame and its morphological opening and closing, which amounts to a doubling of the image intensity values followed by a subtraction of both the opened and closed images.

$$PS(I,S) = \left(I - (I \bullet S)\right) + \left(I - (I \circ S)\right) \quad (6)$$

$$PS(I,S) = 2I - (I \bullet S) - (I \circ S) \quad (7)$$

In this manner, positive features generate a positive-value response and negative features generate a negative response. Thus, information regarding the polarity of detected features is maintained at the expense of minor computational burden (essentially a left-shifting of image intensity values and an additional image subtraction). As with the previous approach, a dual-filter configuration was implemented in order to reduce the probability of false detections due to jagged boundaries on larger clutter.

While morphological filtering is effective at detecting small target signals, it is also susceptible to false detections due to random noise on individual pixels. The output of the morphological filter is thus passed through a dynamic programming algorithm, which reduces the effects of random noise as discussed in the following section.

B. Dynamic Programming

The dynamic programming algorithm averages the image sequence of morphological filter outputs along possible target trajectories, with a decision on the presence of targets being made only after the summation of multiple frames. The number of possible target trajectories can be reduced by considering the possible target state transitions between consecutive frames.

A target signal in an image frame may be represented by a $-1 \le u,v \le 1$ state (i,j,u,v), consisting of a 2D image position (i,j) and a 2D image velocity (u,v). The velocity space is discretized and limited to the range of possible target velocities, with separate branches in the dynamic programming algorithm used to process each possible (u,v). For the problem of airborne collision avoidance, the near-stationary nature of the target signal [19] allows us to limit the discrete velocity space to pixels per frame. This corresponds to a continuous target velocity of anywhere between 0 and ±1 pixels per frame. The discrete position space (i,j) corresponds to the row-column index of pixels in each frame.

Assuming velocity is constant, it can been shown [14] that for each discrete target state (i,j,u,v) at frame k, there are 4 possible state transformations corresponding to frame k+1. Given the velocity space for this problem, four velocity branches are sufficient to accommodate possible target

motion. Their ranges of valid state transformations are shown in Fig. 1.

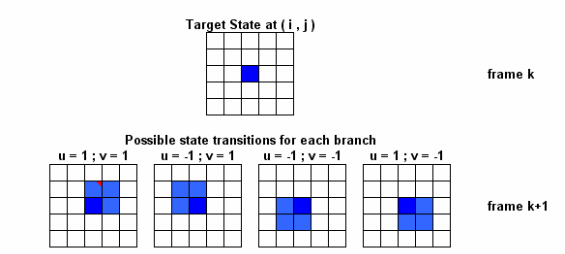

Fig. 1 Possible State Transitions for Dynamic Programming Algorithm.

The dynamic programming implementation used in this paper is based on the approach of Yang [16]. The algorithm is divided into three stages – Initialisation, Recursion, and Decision.

Initialisation

An intermediate merit function, $F_{uv}(i,j,k)$ which recursively tracks possible target states on a frame-to-frame basis is created for each discrete velocity branch and initialized with a value of zero.

For all (u,v):

$$F_{uv}(i,j,0) = 0 \tag{8}$$

Recursion

The merit function for frame *k* is defined as a weighted sum of the current incoming frame and a value taken from the previous merit function at frame *k-1*. More specifically, the latter value is the maximum response from the four-pixel window of valid state transitions for target state (i,j,u,v).

For all (u,v):

$$F_{uv}(i,j,k) = \left[(1-\alpha) f(i,j,k)\right] + \left[\alpha \times \max_{(i',j') \in Q(i,j,u,v)} F_{uv}(i',j',(k-1))\right] \tag{9}$$

Where:

$f(i,j,k)$ is the filtered image received at frame *k*

$0 \le a \le 1$ represents a memory factor

$Q(i,j,u,v)$ represents the four-pixel window of valid rearward transitions for target state (i,j,u,v).

Since this addition is performed recursively, $Q(i,j,u,v)$ is equivalent to the reflection around (i,j) of the possible *forward* transitions which are shown in Fig. 1.

Decision

At frame K, the maximum output on a pixel-to-pixel basis is taken from the four discrete velocity branches.

$$F_{\max}(i,j,K) = \max_{(u,v)} F_{uv}(i,j,K) \tag{10}$$

This output may be converted to a binary image with the threshold τ set to achieve appropriate probabilities of detection and false alarm.

The algorithm described above is designed to detect positive-value responses extracted from the initial morphological filtering stage, and will suffice for the simpler CMO approach described previously. However, the alternative preserved-sign approach may contain negative-value responses which would be suppressed by the max filter during the recursion stage of the dynamic programming algorithm.

In order to accommodate these negative-value responses, a separate implementation of the above algorithm may be processed in parallel, slightly modified in that the incoming frame $f(i,j,k)$ is multiplied by -1 during the recursion phase before addition. Detection of positive and negative features may then be combined using a logical OR on a pixel-to-pixel basis.

III. Data Collection

The camera used for this series of trials was a PointGrey Research Dragonfly. Designed specifically for industrial machine vision tasks, the Dragonfly communicates via an IEEE1394 IIDC interface and is capable of producing a colour (Bayer tiled) or greyscale image of up to 1024x768 pixels. The camera was equipped with a Pentax C-Mount lens with a field of view (FOV) of approximately 17° x 13°, an aperture set to f/8 and focus set to infinity.

A sensor platform was constructed, consisting of the Dragonfly camera and lens, a GPS receiver, and an inertial measurement unit [20] which was used to measure camera pose. This was mounted atop a ridge near Mary Cairncross Reserve, a location with an elevation of approximately 1000ft, around 2nmi SE from the township of Maleny.

From this location, a series of image streams were recorded featuring a target aircraft that was made to fly on a direct collision course with the sensor platform for a period of time, before gradually pulling away to maintain safe distance from terrain. For comparative purposes, an 'alerted' human observer was present at the site and was made to record the times at which the target aircraft could be detected via the human visual system. This observer was equipped with binoculars to allow precise determination of target bearing before attempting to locate the aircraft with the naked eye. It should be noted that this represents a very favourable estimate of human "see and avoid" performance. In a typical real-life cockpit scenario, much of the pilot's time is spent performing a thorough scan for traffic, a factor which as been identified as one of the major limitations of the "see and avoid" principle [19].

In each of the trials, data from the camera was recorded at a frame rate of 7.5 Hz using the Linux-based program Coriander and later processed offline. A log of GPS location onboard the target aircraft was also recorded in order to determine the range at which the target aircraft could be

detected, by either the image processing algorithms or the human observer.

IV. Results and Analysis

The target detection algorithms described previously were used to process the data collected from the field trials, with the memory factor α set to a value of 0.75 and the threshold value τ varied to compare the subsequent effect on detection performance. Results presented in this section describe the transformation of an image frame as it passes though the morphological CMO filter and subsequent dynamic programming and thresholding phases. Comparisons are made against the performance of the alerted human observer, and between the performances of the two morphological filtering approaches in terms of false alarm rates and detection times.

A. Target Detection Example: CMO Approach

The effect of each intermediate phase of the close-minus-open detection algorithm is demonstrated via the images shown in Fig. 2. Represented in these images is a small window taken from one of the recorded image frames, featuring a target aircraft in the bottom right corner against a background of cloud clutter. For viewing purposes, the outputs displayed in Fig. 2(b) and (c) have been gamma-corrected with a factor of 0.25 to enhance the detail present in the dark images. Brighter areas in the outputs of the CMO filter and dynamic programming responses indicate the possible presence of targets. Fig. 2(d) corresponds to the binary conversion of the dynamic programming output with a fixed threshold of 0.030 (on a 0-1 brightness scale).

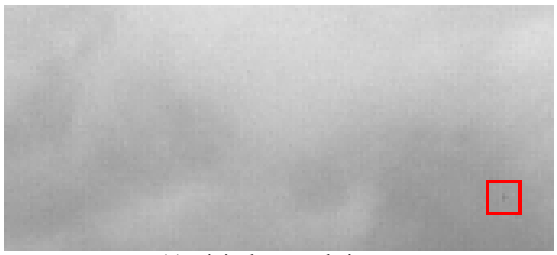

(a) original grayscale image

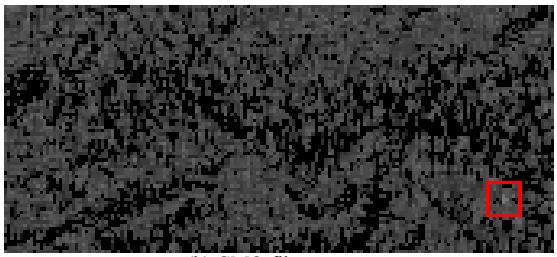

(b) CMO filter output

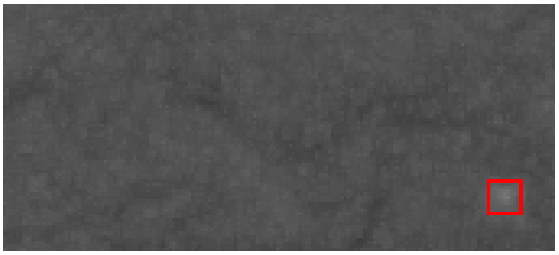

(c) dynamic programming output

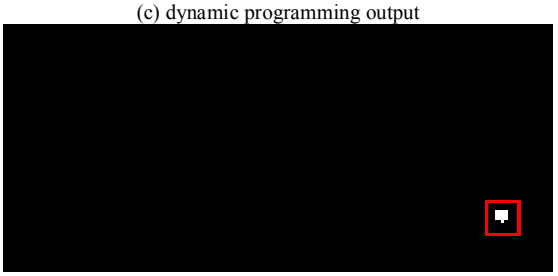

(d) binary output with threshold $\tau = 0.030$

Fig. 2 Image outputs at different stages of the target detection algorithm

As can be seen, the output of the morphological CMO filter shown in Fig. 2(b) has extracted point-like features from the greyscale image frame. There is a particularly strong feature, surrounded by the red box, which corresponds to the target signal. However, there are also numerous other features of similar strengths that correspond to noise on individual pixels. A threshold decision made at this point in the algorithm would be overly susceptible to false alarms due to such noise. Hence, this output is subject to dynamic programming before a decision is made on target presence.

Fig. 2(c) shows that the dynamic programming algorithm has averaged out the effects of noise while maintaining the strength of the target signal. Note that the edges of the target appear less defined as a result of the recursive phase of the dynamic programming algorithm. Non-maxima suppression could be used if single-point detection is desired, however it was not necessary for this experiment. The binary conversion of the dynamic programming output serves as the final decision on the presence of a target, and is observed in Fig. 2(d) to have successfully detected the genuine target while suppressing potential false alarms due to image noise.

B. Comparison Against Human Detection Performance

One of the major goals of this research is to demonstrate a target detection algorithm that achieves a level of performance which is equivalent or superior to that of a human pilot. In this section, comparisons are made between the detection times and corresponding distances achieved by the algorithms described previously and those recorded by the alerted human observer. Detection times are presented in terms of frame index, or approximate frame index in the case of the human observer. Detection distances were calculated using GPS data, which was collected both onboard the target aircraft and at the test location.

Table I presents a performance comparison for one of the recorded image streams, denoted *Stream A*. This dataset was captured in bright lighting conditions and features a background of heavy cloud clutter and natural terrain. The

target detection algorithm featured in this comparison is the CMO approach, with parameters α=0.75 and τ=0.035.

As can be seen in Table I, the target is first detected by the algorithm at a distance of 6.7km, 36.7% greater than the distance achieved by the alerted human observer. However, consistent detection is arguably a more meaningful performance metric, since at this point a subsequent tracking algorithm may be used to distinguish genuine threats from residual false alarms due to point-like clutter (e.g. distant houses, individual trees etc.). This is defined as the point at which no missed detection frames are encountered for the remainder of the collision scenario, and is achieved at a distance of 6km, 22% further than that of the first human observation.

TABLE I
COMPARISON AGAINST HUMAN DETECTION PERFORMANCE: IMAGE STREAM A

	Frame #	**Target Distance (km)**
First Detection	56	6.7 (3.6 nmi)
Consistent Detection	164	6.0 (3.2 nmi)
Human Observer Detection	273 (approx)	4.9 (2.6 nmi)

Table II presents a performance comparison, using the same algorithm with identical parameters, for another of the recorded image streams, denoted *Stream B*. This dataset was captured in dimmer lighting conditions than in *Stream A*, with a similar background. In this example, the target was first detected at a distance of 6.6km, approximately 40.4% greater than the first human observation. Consistent detection was achieved at a target distance of 5.6km, 19% further than the human detection distance. Note that the distances required for successful detection, both for the computer vision algorithm and the human observer, are slightly shorter for *Stream B* than in *Stream A*. This is due to the decrease in target contrast as a result of the dimmer lighting conditions.

TABLE II
COMPARISON AGAINST HUMAN DETECTION PERFORMANCE: IMAGE STREAM B

	Frame #	**Target Distance (km)**
First Detection	83	6.6 (3.56 nmi)
Consistent Detection	258	5.6 (3.0 nmi)
First Human Detection	333 (approx)	4.7 (2.5 nmi)

C. Comparison of Morphological Filtering Approaches

In this section, performance comparisons based on four key criteria are made between the close-minus-open and the preserved-sign approaches. These criteria are the total rate of false alarms, the rate of intermittent false alarms, the times of first detection and the times of consistent detection. Intermittent false alarms are defined as incorrect target detections that do not appear on consecutive frames. These are presented separately to the overall rate of false alarms in order to exclude persistent responses due to point-like clutter. As defined previously, consistent detection is the point at which no missed detection frames are encountered for the remainder of the collision scenario.

For the most effective comparison, a dataset was chosen featuring a relatively smooth background in an effort to reduce the number of false alarms due to point-like clutter. As a consequence, the rate of false alarms, particularly at lower detection thresholds, is dominated by image noise and the results achieved by the preserved-sign morphological filter become more evident.

This dataset was processed by the target detection algorithms, with the memory factor α set to 0.75, and the detection threshold τ varied between 0.025 and 0.035 in order to investigate the resulting effects on performance. Table III presents a summary of results for comparison.

Note that a significant number of false alarms are generated by both algorithms, even at higher values for detection threshold τ. These will be suppressed in a subsequent feature tracking stage, whereby genuine collision threats are identified based on characteristics such as a low rate of image translation and a high rate of image expansion [2].

TABLE III
COMPARISON BETWEEN MORPHOLOGICAL FILTERING APPROACHES

	τ	CMO Approach	PS Approach	% Change
First Detection (Frame #)	0.025	5	5	-
	0.030	20	20	-
	0.035	53	53	-
Consistent Detection (Frame #)	0.025	144	144	-
	0.030	171	171	-
	0.035	190	190	-
Total False Alarms / Frame	0.025	15.9	11.9	-24.8%
	0.030	4.86	4.85	-0.3%
	0.035	2.62	2.62	-
Intermittent False Alarms / Frame	0.025	4.82	1.4	-70.9%
	0.030	0.585	0.60	2.5%
	0.035	0.34	0.34	-

The upper half of Table III shows that the first detection and consistent detection frame numbers are equivalent, thus indicating that detection sensitivity is not affected by the implementation of the preserved-sign approach. The lower half of Table III provides a performance comparison between the approaches in terms of the total number of false alarms per frame and the number of intermittent false alarms per frame, averaged over 200 frames. As anticipated, the preserved-sign approach performed very well in comparison to the CMO approach at the lower threshold value of 0.025, achieving a

70.9% reduction in intermittent false alarms. At this threshold level, the CMO algorithm is particularly susceptible to false alarms, since they can easily be generated by zero-mean noise. The non-negative nature of the CMO output means that such noise is no longer characterised by a zero mean, thus reducing the effectiveness of subsequent temporal averaging via the dynamic programming algorithm.

The change in false alarm rates between the two approaches becomes negligible as the threshold value is increased to the point where image noise alone is unlikely to generate false alarms. In this case, the majority of false alarms take the form of persistent responses generated as a result of strong, point-like clutter, or intermittent responses due to weaker clutter with the coherent addition of noise. Because such responses are primarily influenced by the presence of clutter, they are characterised by a non-zero mean and are unlikely to change sign over multiple frames, diminishing the impact of preserving the sign of detected features.

V. Conclusions & Future Work

This paper has presented a comparison of two image processing target detection algorithms with a view to developing UAV "sense and avoid" capabilities.

Comparisons were made between the performance of the detection algorithms in processing a real-life collision scenario, and that of an alerted human observer present at the test site. Results indicated that the target could be first detected at ranges 35-40% greater than those measured from the human observer, even amongst heavy cloud clutter. Such results are important, given current "sense and avoid" regulatory requirements for a level of performance equivalent or superior to that of a human pilot [7].

Comparisons were also made between the two morphological filtering approaches in terms of detection times and false alarm rates. Results have shown that, while little difference can be observed between the two approaches at higher values of detection threshold, the preserved-sign approach offers greater resilience to noise-based false alarms as the detection sensitivity is increased. This advantage does, however, come at the expense of additional computational burden, specifically an extra subtraction and left shift operation for each pixel during morphological filtering and a separate, parallel implementation of the dynamic programming algorithm for the identification of negative targets.

In future work, the scope of this research will be broadened to include a post-detection feature tracking stage, where genuine collision threats are distinguished from residual false alarms. This will be based on characteristics such as a low rate of image translation coupled with a high rate of image expansion [2]. Additionally, the eventual use of cameras onboard moving platforms will require the development of a strategy to compensate for ego-motion effects. This may be achieved through integration with inertial sensors.

Ultimately, this research endeavours to develop a computer vision based system that delivers appropriate UAV "sense and avoid" capabilities under a wide range of scenarios, including variations in lighting, weather and background conditions. Such a system would make a significant contribution towards the large-scale introduction of UAV technology for use in civilian applications.

References

[1] NASA, "Researchers encouraged by collision avoidance test results," in *NASA Dryden Flight Research Centre News Release 03-21*, 2003.

[2] T. Gandhi, M.-T. Yang, R. Kasturi, O. Camps, L. Coraor, and J. McCandless, "Detection of obstacles in the flight path of an aircraft," *Aerospace and Electronic Systems, IEEE Transactions on*, vol. 39, pp. 176-191, 2003.

[3] W. H. Harman, "TCAS: A system for preventing midair collisions," *The Lincoln Laboratory Journal*, vol. 2, 1989.

[4] Y. Ikeda, B. Nguyen, A. Barfield, B. Sundqvist, and S. Jones, "Automatic air collision avoidance system," presented at SICE 2002. Proceedings of the 41st SICE Annual Conference, 2002.

[5] R. Holdsworth, J. Lambert, and N. Harle, "Inflight path planning replacing pure collision avoidance, using ADS-B," *Aerospace and Electronic Systems Magazine, IEEE*, vol. 16, pp. 27-32, 2001.

[6] R. Y. Gazit and J. D. Powell, "Aircraft collision avoidance based on GPS position broadcasts," presented at Digital Avionics Systems Conference, 1996., 15th AIAA/IEEE, 1996.

[7] Federal Aviation Administration, "Chapter 12, Section 9, Remotely Operated Aircraft," in *Order 7610.4: Special Military Operations*. Washington D.C., USA: US Government Printing Office.

[8] D. Casasent and A. Ye, "Detection filters and algorithm fusion for ATR," *Image Processing, IEEE Transactions on*, vol. 6, pp. 114-125, 1997.

[9] N. Sang, T. Zang, and G. Wang, "Gray scale morphology for small object detection," *SPIE 2759 Signal and data procession of small targets*, pp. 123-129, 1996.

[10] S. D. Deshpande, M. H. Er, R. Venkateswarlu, and P. Chan, "Max-mean and max-median filters for detection of small targets," presented at Signal and Data Processing of Small Targets 1999, 1999.

[11] Zhanghong, Zhaobaojun, and Maoerke, "A real-time effective method for infrared point-target detection in spatially varying clutter," presented at Radar, 2001 CIE International Conference on, Proceedings, 2001.

[12] I. S. Reed, R. M. Gagliardi, and L. B. Stotts, "Optical moving target detection with 3-D matched filtering," *Aerospace and Electronic Systems, IEEE Transactions on*, vol. 24, pp. 327-336, 1988.

[13] M. Diani, G. Corsini, and A. Baldacci, "Space-time processing for the detection of airborne targets in IR image sequences," *Vision, Image and Signal Processing, IEE Proceedings-*, vol. 148, pp. 151-157, 2001.

[14] S. M. Tonissen and R. J. Evans, "Target tracking using dynamic programming: algorithm and performance," presented at Decision and Control, 1995., Proceedings of the 34th IEEE Conference on, 1995.

[15] Y. Barniv, "Dynamic programming solution for detecting dim moving targets," *IEEE Transactions on Aerospace and Electronic Systems*, vol. AES-21, 1, 1985.

[16] M.-T. Yang, T. Gandhi, R. Kasturi, L. Coraor, O. Camps, and J. McCandless, "Real-Time Implementations of Obstacle Detection Algorithms on a Datacube MaxPCI Architecture," *Real-Time Imaging 8*, pp. 157-172, 2002.

[17] K.-I. Nishiguchi, M. Kobayashi, and A. Ichikawa, "Small target detection from image sequences using recursive max filter," presented at Signal and Data Processing of Small Targets 1995, San Diego, CA, USA, 1995.

[18] R. C. Warren, "Detection of Distant Airborne Targets in Cluttered Backgrounds in Infrared Image Sequences," PhD. Dissertation, University of South Australia, Adelaide, Australia, 2002.

[19] Bureau of Air Safety Investigation, "Limitations of the See-and-Avoid Principle," 1991.

[20] J. M. Roberts, P. I. Corke, and G. Buskey, "Low-cost flight control system for a small autonomous helicopter," presented at Australasian Conference on Robotics and Automation, Auckland, 2002.